Received April 27, 2021, accepted May 17, 2021, date of publication May 31, 2021, date of current version March 14, 2022.

Digital Object Identifier 10.1109/ACCESS.2021.3084892

Preliminary Evaluation of Induction Switched Reluctance Machine (ISRM) for Electric Vehicle Application

MEYSAM AZAMIAN JAZI[1], MOHAMMADALI ABBASIAN[1], AND DIETER GERLING[2], (Member, IEEE)

[1]Department of Engineering, Islamic Azad University, Isfahan (Khorasgan) Branch, Isfahan 39998-81551, Iran
[2]Institute for Electrical Drives and Actuators, Bundeswehr University Munich, 80797 Neubiberg, Germany

Corresponding author: Mohammadali Abbasian (m.abbasian@khuisf.ac.ir)

ABSTRACT In this paper, a novel electric machine, Induction Switched Reluctance Machine (US patent-US20170370296A1) is introduced, and its preliminary performance is evaluated. The innovation is based on placing windings on the rotor, in order to create short magnetic flux paths in the rotor and stator core of the electric machine. As a result, a higher torque with lower copper and iron losses is generated. Like other ideas, there are unknown aspects of this electric machine, such as thermal and mechanical properties, that should be studied. A comprehensive research program is required to analyze and design an Induction Switched Reluctance Machine with an optimized configuration. This electric machine could be designed with different pole numbers and various winding strategies, and it is not possible to consider all configurations and aspects of it in this paper. Moreover, the size and the rated power of the machine can affect its properties. The purpose of this paper is to introduce, simulate and prototype a simple Induction Switched Reluctance Machine. This electric machine has an excellent potential to be implemented in the propulsion system of electric vehicles.

INDEX TERMS Reluctance machines, electromagnetic induction, torque, electric vehicle.

I. INTRODUCTION

Internal combustion engines have been operating as traction motors in different vehicles for decades. Because of the drawbacks of these engines, such as having low efficiency and being the primary source of air pollution, they will be replaced by electric machines [1]. Designing electric motors for electric vehicle propulsion systems, can profoundly affect the properties of the vehicle. For instance, the power, torque, speed, efficiency, noise, vibration, speed range, reliability, robustness, fault tolerance and cost of the electric traction motor can determine the overall properties of the vehicle [2].

There are several candidates to be implemented as traction motor in electric vehicles. The most popular option is Interior Permanent Magnet Synchronous Machine (IPMSM), which has high efficiency and excellent torque density [3]–[7].

Actually, IPMSM is not an ideal option for electric vehicle propulsion systems. The high efficiency and excellent power density of IPMSM are due to the rotor-mounted rare-earth materials, such as NdFeB and SaCo. High cost, supply limit, and demagnetization risks are the main drawbacks of the mentioned permanent magnets (PMs) [8].

Induction Machine (IM) is another important candidate for electric vehicle application. IM has acceptable power density, but it suffers from lower efficiency compared to IPMSM. The conductors on the rotor of IM are significant sources of ohmic loss of the machine [7], [8].

There are two categories of electric machines that are free of PMs and conductors on the rotor: Switched Reluctance Machines (SRMs) and Synchronous Reluctance Machines (SynRMs). In these machines, the reluctance torque is responsible for the motor rotation. These reluctance-based motors cannot generate torque as much as PM-based motors, but their structure is very simple [9].

SRMs suffer from low torque density, and high level of noise and vibration. In recent decades, overwhelming efforts have been deployed to design better SRMs, and several new SRMs have been introduced [10]–[16]. For instance,

The associate editor coordinating the review of this manuscript and approving it for publication was Feifei Bu.

Segmented Switched Reluctance Machine (SSRM) was presented in 2004 [13]. In this topology, the rotor comprises several ferromagnetic segments (rotor poles). Because of a segmented structure, the magnetic flux cannot circle the entire yoke of the stator and a short flux path is achieved. SSRMs can also have a segmented stator and a non-segmented rotor [15]. Different configurations of SSRMs have been presented till now, and their higher torque compared to conventional SRMs has been highlighted as an important advantage.

A SSRM can generate 40 percent more torque compared to a same-dimension conventional SRM [13]. But manufacturing a segmented rotor or stator can cause practical problems. Even the slightest deviation in the assembling process of SSRM can unbalance the radial forces of the rotating machine, which emerges as a source of vibration [16]. Moreover, this assembling process is the major obstacle to achieving a very small airgap between the rotor and the stator of SSRM (less than 0.5 mm). Actually, the airgap of a conventional SRM (without segmented rotor and stator), can be smaller than the airgap of a SSRM. As a result, a conventional SRM may have more torque density compared to a SSRM.

Another high torque SRM, Double Stator Switched Reluctance Machine (DSSRM) was introduced for electric vehicle application in 2010 [16]. In this machine, a hollow cylindrical rotor is sandwiched between two stators. Similar to SSRM, the segmented rotor in DSSRM guaranties the short flux paths. DSSRM's torque density is two times more than conventional SRM. But DSSRM has a complicated configuration, and it is difficult to assemble this double stator electric machine.

Short flux path SRMs, such as SSRM and DSSRM, have lower iron loss at high speeds. More importantly, short flux path SRMs may have higher torque density and lower vibration [16].

Obtaining a short flux path in a non-segmented rotor and stator is a very important objective for SRM designers. By implementing conductors on the rotor, this goal may be achieved. Based on the Faraday's law of induction, the conductors on the rotor can influence the magnetic flux path, and orient it in the desired direction. Placing the conductors in a right position, with a proper arrangement and connection, is the essential issue in this problem. In this paper, this idea is presented, and Induction Switched Reluctance Machine (ISRM) is introduced.

As will be discussed in this paper, a short magnetic flux path is achieved in ISRM, while there is no segmented rotor or segmented stator in the machine. This is an important advantage that can result in high efficiecny, high torque density and high power density. On the other hand, having conductors on the rotor is a drawback to this electric machine. This can cause mechanical problems and overheating. Moreover, ISRM has high torque ripple. In this paper some of these issues will be addressed.

ISRM can be designed in different topologies and various pole numbers. In this paper an ISRM with 12 stator poles and 8 rotor poles is presented for electric vehicle application. Then it is modeled using 2D Finite Element Method (FEM), and compared with a conventional SRM in terms of torque capability, copper loss and torque ripple. Finally, a prototype of a low-power ISRM and its appropriate electric drive is built, and the experimental results are presented.

II. INDUCTION SWITCHED RELUCTANCE MACHINE

Induction Switched Reluctance Machine (ISRM) is a novel electric machine with one stator, one rotor and several short-circuited coils which are disposed on the rotor [17]. The machine is excited by separate coils which are placed in the stator slots. The short-circuited coils on the rotor are not excited by any external power source, but the current is induced in the rotor conductors. The arrangement of the windings of the rotor is formed in a particular way that finally a short flux path is created around the excited stator coil.

A. CONFIGURATION OF ISRM

ISRM can be designed in various configurations with different stator and rotor pole numbers. Depending on the configuration, short-pitched or full-pitched coils are required. In some configurations, both the stator and the rotor coils are full-pitched. In some other configurations, both the stator and the rotor coils are short-pitched. But in some configurations the stator coils are full-pitched and the rotor coils are short-pitched [17].

Various configurations of ISRM should be studied in order to determine its potential to be used in electric vehicles. In this paper, one of the ISRM topologies with 12 stator poles and 8 rotor poles is chosen to be studied. This ISRM has full-pitched coils on the stator, and short-pitched coils on the rotor. The cross-section of this 12/8 ISRM is illustrated in Fig. 1.

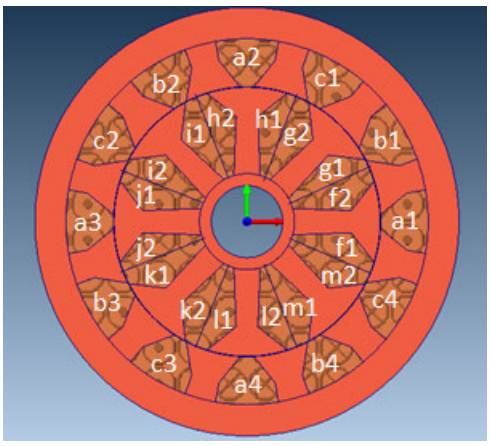

FIGURE 1. The cross-section of a 3-phase 12/8 ISRM.

In this three-phase ISRM, there are two coils per phase which are connected in series. For instance, a_1a_2 and a_3a_4 are connected together and form phase A. This is also the case for phase B and phase C. Each stator coil is made up of concentrated windings. On the rotor side, one isolated short-circuited concentrated winding is coiled around each

rotor pole (f_1f_2, g_1g_2, ...). The stator winding connections of ISRM is shown in Fig. 2.

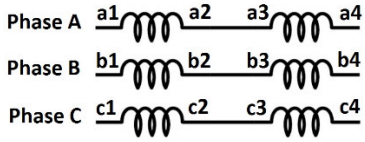

FIGURE 2. The stator winding connections of a 3-phase 12/8 ISRM.

At first glance, ISRM may look like an Induction Machine (IM). But there are some differences between ISRM and IM. In ISRM, each rotor coil must be disconnected from other rotor coils. The stator and the rotor pole numbers of ISRM are chosen based on the conventional SRM design methods, and the torque profile of ISRM is similar to conventional SRMs. Pulsed DC is used for phase excitation of ISRM, and a very short magnetic flux path is created around the stator windings of ISRM, which is different from the magnetic flux distribution of IM.

According to Faraday's law of induction, when a phase of ISRM is excited and the rotor is rotating, the magnetic field in the short-circuited rotor coils changes over time, and electromotive force (EMF) is produced. The direction of EMF and the induced current in the rotor windings can be determined by Lenz's law. The outcome is that the resultant flux lines are prevented to enter the rotor back iron and a very short flux path is created around the excited stator phase. In this paper, this phenomenon in ISRM is investigated using Finite Element Method (FEM), and the results are presented.

B. ISRM EQUATIONS

The mathematical model of ISRM is highly nonlinear due to influence of the magnetic saturation. In this section, some essential equations of ISRM are derived.

Like conventional SRMs, the rotor stroke angle for ISRM is [18]:

$$\theta_{st} = \left| \frac{2\pi}{N_s} - \frac{2\pi}{N_r} \right| \tag{1}$$

where N_s is the number of stator poles, and N_r is the number of rotor poles. The phase voltage equation for ISRM is:

$$v = R_s i + \frac{d\varphi\,(i,\theta)}{dt} \tag{2}$$

where v is the phase voltage, R_s is the stator phase resistance, i is the phase current, φ is the stator phase total magnetic flux linkage (considering the mutual flux of the rotor coils), and θ is the rotor angle.

Rewriting the phase voltage equation in terms of partial derivatives yields this equation:

$$v = R_s i + \frac{\partial\varphi}{\partial i}\frac{di}{dt} + \frac{\partial\varphi}{\partial\theta}\frac{d\theta}{dt} \tag{3}$$

L_{eq} is the equivalent stator phase incremental inductance, considering the mutual flux of the rotor coils. L_{eq} is defined as:

$$L_{eq} = \frac{\partial\varphi}{\partial i} \tag{4}$$

TABLE 1. Characteristics of the machines (ISRM and SRM).

Stator Outer Radius	115 mm
Stack length	90 mm
Airgap	0.5 mm
Number of stator poles	12
Number of rotor poles	8
Turn number of stator coils	40
Turn number of rotor coils (only for ISRM)	40
Rated current	200 A
Maximum current density	20 A/mm^2
Rotor and stator material	M19
Rated power (ISRM)	100 kW
Rated power (SRM)	50 kW
Motor length (ISRM)	209 mm
Motor length (SRM)	131 mm
Cooling method	Oil spray cooling

Actually, L_{eq} represents the resultant of the excited stator coil flux, and the flux due to the magnetic coupling between the excited stator coil and the rotor coils.

Rotor speed (ω_r), and back electromotive force (e) are defined as:

$$\omega_r = \frac{d\theta}{dt} \tag{5}$$

$$e = \frac{\partial\varphi}{\partial\theta}\omega_r \tag{6}$$

Substituting these terms into the rewritten voltage equation yields this voltage equation:

$$v = R_s i + L_{eq}\,(i,\theta)\,\frac{di}{dt} + e \tag{7}$$

The coenergy of the magnetic field is obtained as [18]:

$$W'\,(\theta, i) = \int_0^i \varphi\,(\theta, i)\,di \tag{8}$$

The generated torque is determined by differentiating $W'(\theta, i)$ with respect to θ at constant current:

$$T = \left.\frac{\partial W'}{\partial\theta}\right|_{i=constant} \tag{9}$$

If ISRM is not saturated, the expression for torque can be derived, and is given by:

$$T = \frac{1}{2}i^2\frac{dL_{eq}}{d\theta} \tag{10}$$

C. FINITE ELEMENT ANALYSIS OF ISRM

In order to probe the effect of short-circuited windings around the rotor poles, a 2D model of an ISRM with the characteristics presented in Table 1 is created. Firstly, it is assumed that there is no winding around the rotor poles of the ISRM; and phase A is excited while the rotor is rotating at the speed of 2500 rpm. This model is simulated using transient FEM in MagNet Infolytica, and the magnetic flux lines are calculated and drawn as contour lines (see Fig. 3). The magnetic flux paths in this configuration are distributed all over the machine, and all the rotor and stator poles are occupied.

On the next step, the short-circuited copper coils are added to the rotor of the ISRM, as illustrated in Fig. 1. Then the

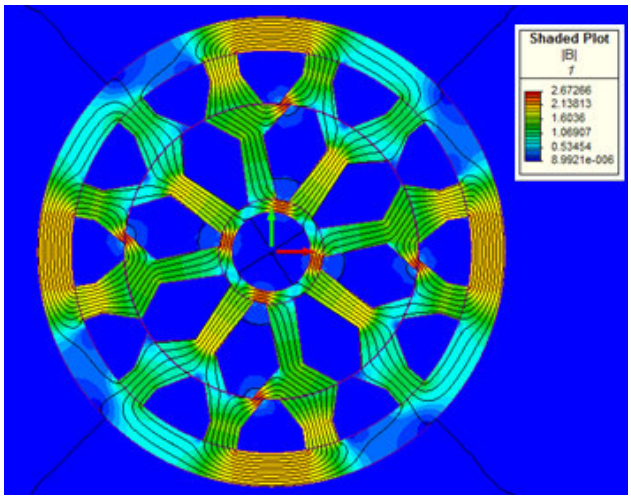

FIGURE 3. The flux distribution in the proposed machine without rotor windings.

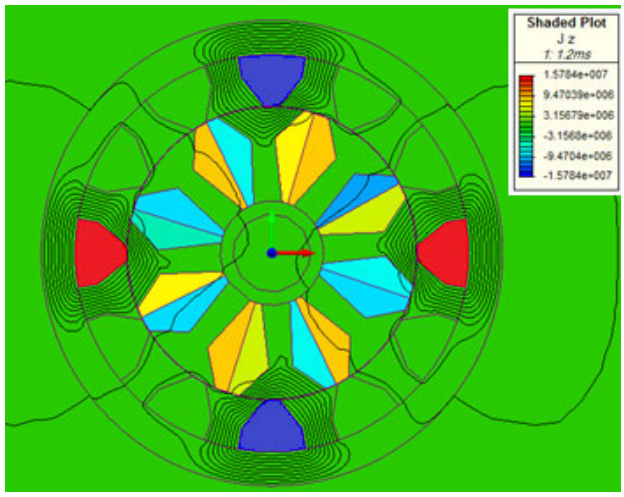

FIGURE 4. The current distribution in the ISRM coils when phase A is excited.

transient FEM simulation of the ISRM is accomplished. The current of phase A is constant and the rotor runs at the speed of 2500 rpm. Fig. 4 shows the distribution of the phase A current. Moreover, the induced currents in the rotor windings are observable in this figure. Fig. 5 illustrates the resultant flux distribution in the ISRM as contour lines. Regarding the previous discussion, a very short flux path is created around the excited stator phase.

D. TORQUE CHARACTERISTICS OF ISRM

Since there is no source of electromagnetic field on the rotor of conventional SRMs, only reluctance torque is generated in that electric machines. But in ISRM, there are windings on the rotor which carry the induced current, and this will affect the resultant torque. Actually, the time-varying electromagnetic field interacts with the rotor coil currents, and induction torque is produced. As a result, both reluctance torque and induction torque play a role in torque generation. To have a better vision about the torque properties of ISRM, a transient FEM analysis is required.

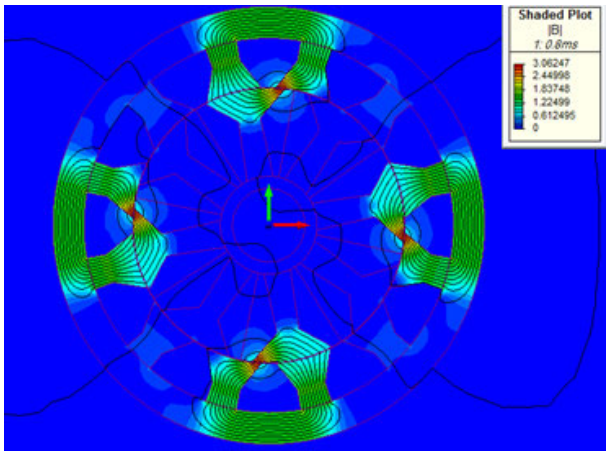

FIGURE 5. The flux distribution in the ISRM when phase A is excited.

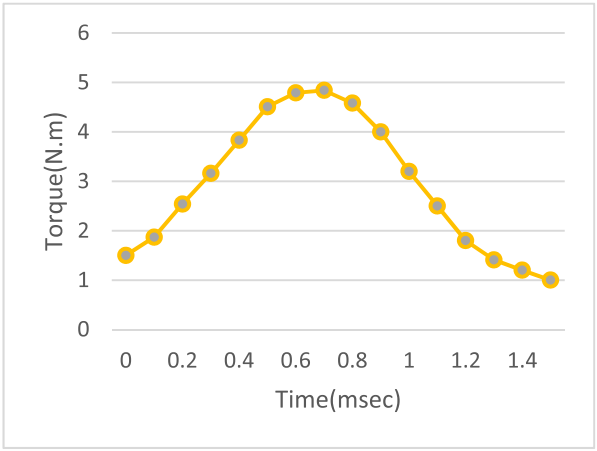

FIGURE 6. The induction torque of the ISRM.

The ISRM with the characteristics presented in Table 1 is considered to be analyzed using transient FEM. In this simulation, it is assumed that phase A is excited, and the phase current is 100 A. The rotor is rotating with the constant speed of 2500 rpm from unaligned position (the rotor position angle is 22.5° at t = 0 msec) to aligned position (the rotor position angle is 0° at t = 1.5 msec).

After solving the FEM model of the ISRM in MagNet, the induction torque (on the rotor windings), the total generated torque, and the dynamic torque of the ISRM is calculated and the final results are presented in Fig. 6, Fig. 7 and Fig. 8, respectively. The results clarify that the induction torque is neglectable and the reluctance torque is the major source of the produced torque in ISRM.

In order to compare ISRM with conventional SRM in terms of torque capability and efficiency, a conventional SRM is considered. The cross-section and the winding connections of a 3-phase 12/8 conventional SRM is shown in Fig. 9 and Fig. 10, respectively. The properties of this SRM which is considered for simulation is presented in Table 1. The dimensions, pole numbers, coil turn numbers, and airgaps of the two motors are equal. A 2D FEM model of the conventional SRM is created and simulated with the same excitation as the ISRM FEM model. In this simulation, it is assumed that

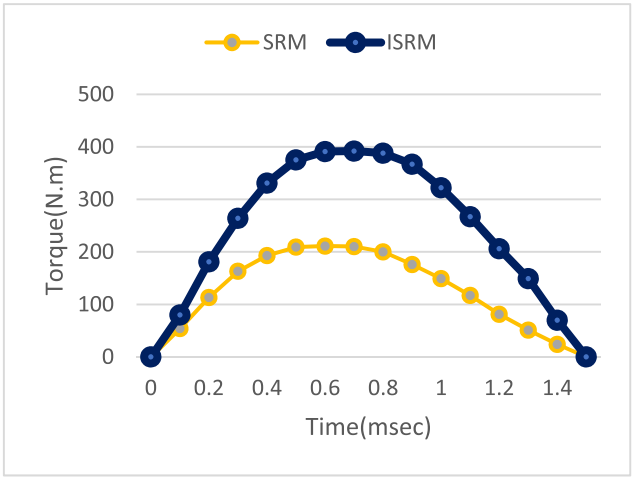

FIGURE 7. The total torque of the ISRM compared to the total torque of the conventional SRM.

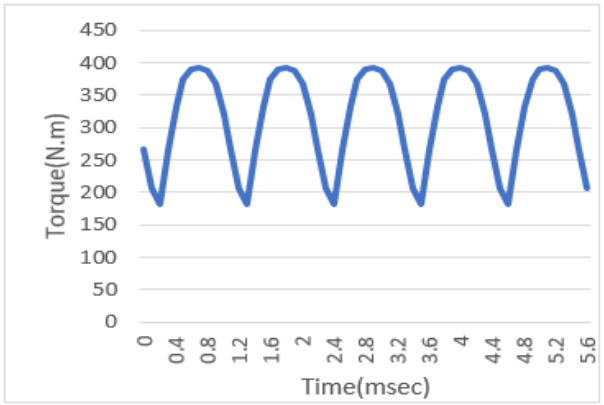

FIGURE 8. The dynamic torque of the ISRM.

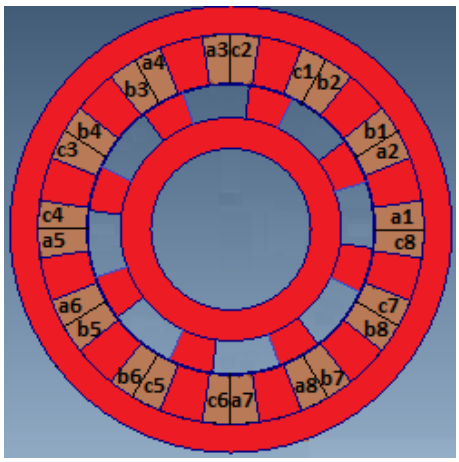

FIGURE 9. The cross-section of a 3-phase 12/8 conventional SRM.

phase A is excited, and the phase current is 100 A. The flux distribution of the conventional SRM is illustrated in Fig. 11. The toque profile of the conventional SRM (along with the torque profile of the ISRM) is shown in Fig. 7.

If the cooling method of these two machines is direct liquid cooling method (such as spray oil cooling) [19], the maximum current density of the conductors can be about 20 A/mm^2 and the maximum phase current will be 200 A.

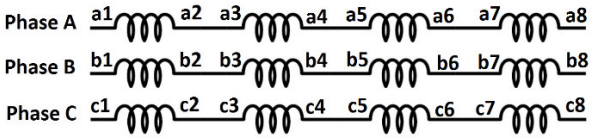

FIGURE 10. The stator winding connections of a 3-phase 12/8 conventional SRM.

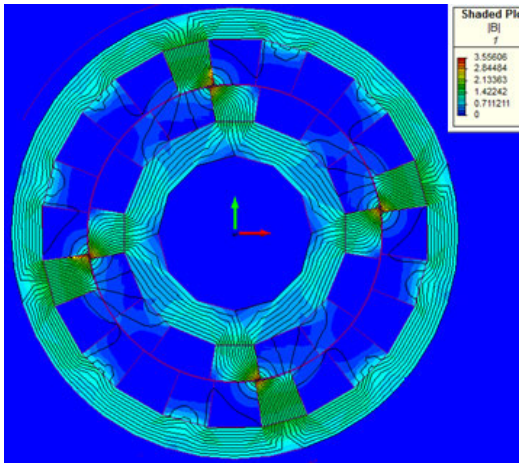

FIGURE 11. The flux distribution in the conventional SRM.

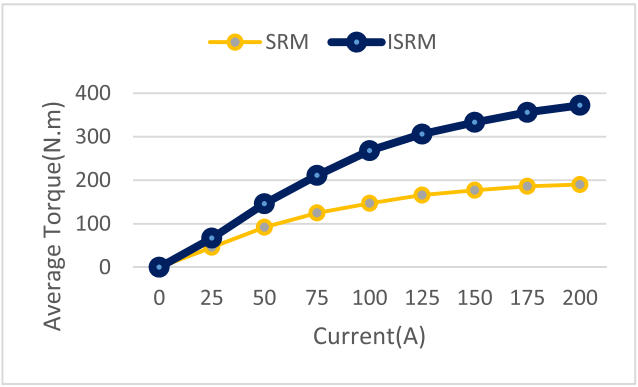

FIGURE 12. The average torque of the ISRM compared to the average torque of the conventional SRM at various phase currents.

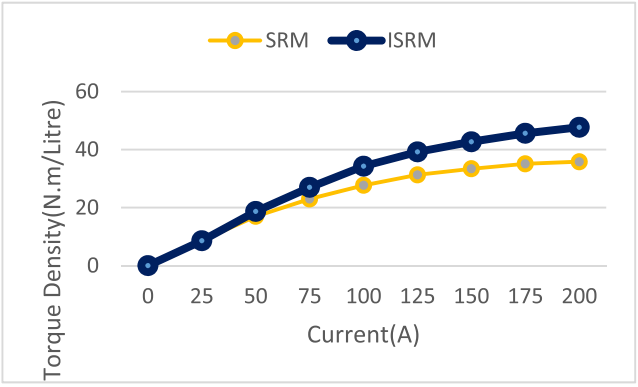

FIGURE 13. The torque density of the ISRM compared to the torque density of the conventional SRM at various phase currents.

In this step, the average torque and the torque density of the ISRM and the conventional SRM are calculated at various phase currents (from 0 A to 200 A), using FEM, and the results are illustrated in Fig. 12 and Fig. 13. The results

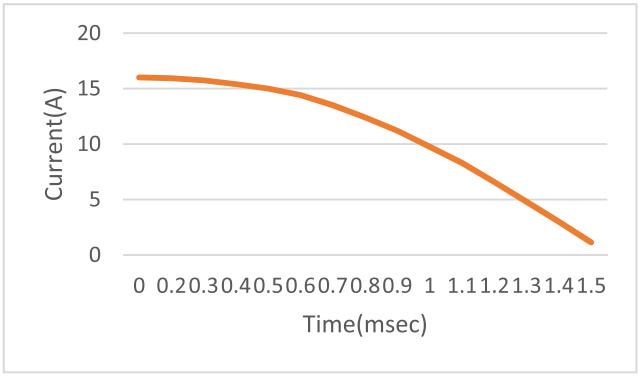

FIGURE 14. The induced current profile in one of the rotor coils.

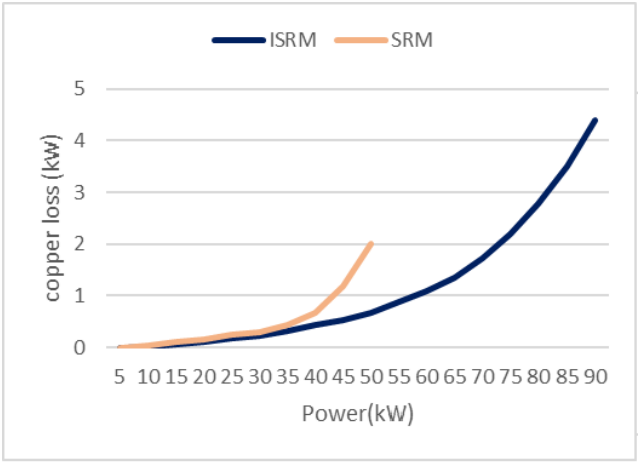

FIGURE 15. The copper loss of the ISRM compared to the copper loss of the conventional SRM at various output powers.

show that ISRM produces more torque, compared to the conventional SRM.

Regarding Fig. 7, the torque profile of ISRM, similar to conventional SRMs, exhibits a high torque ripple. Using the obtained FEM analysis results, the ripple ratio of the machines is calculated for each phase current. The ripple ratio is defined as:

$$(T_{max} - T_{avg})/T_{avg} \tag{11}$$

where T_{max} is the maximum torque, and T_{avg} is the average torque. The calculated ripple ratios are presented in Table 2. The results show that at low torques, the ISRM has higher torque ripple, but at high torques, the ISRM has lower torque ripple, compared to the conventional SRM. ISRM can be driven using conventional SRM electric drives, and the advanced torque ripple reduction techniques can be implemented to ISRM.

E. COPPER LOSS OF ISRM

The induced current in one of the rotor coils of the ISRM is calculated using the FEM model which was created before. In this simulation, the stator phase current is 40 A, and the rotor speed is 2500 rpm. As shown in Fig. 14, larger current is induced in the rotor coils when the rotor is far from the aligned position. When the rotor moves towards the aligned position, the induced current declines. This is a remarkable point, because this helps the rotor coils to experience lower effective current and lower copper loss, compared to the stator coils.

TABLE 2. Calculated ripple ratios of the machines.

Phase current (A)	Average torque of the ISRM (N.m)	Ripple Ratio of the ISRM	Average torque of the SRM (N.m)	Ripple Ratio of the SRM
200	378	0.25	192	0.37
175	351	0.25	187	0.36
150	339	0.26	181	0.36
125	306	0.27	162	0.35
100	269	0.30	149	0.34
75	206	0.35	127	0.32
50	149	0.42	92	0.28
25	64	0.49	51	0.22

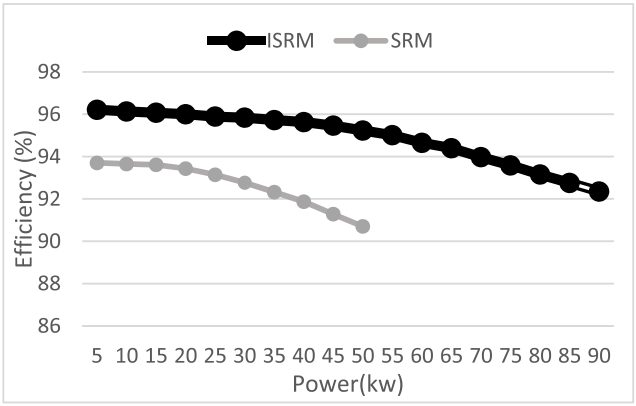

FIGURE 16. The efficiency of the ISRM compared to the efficiency of the conventional SRM at various output powers.

It may be assumed that, because of the windings on the rotor, the copper loss of ISRM is higher than the copper loss of SRM. In order to address this issue, the ISRM and the SRM are analyzed using FEM at various phase currents, and the total copper loss is calculated for each current. The copper losses for different output powers at the speed of 3000 rpm are calculated, and the results are presented in Fig. 15. The copper losses are calculated at the temperature of 70 degrees celsius.

These results show an important fact that the copper loss of the ISRM at each output power is lower than the copper loss of the SRM with the same output power. For example, these two motors have the same copper loss (equal to 1 kW), while the power produced by the ISRM is about 57 kW, and the power produced by the SRM is about 43 kW (See Fig. 15).

These results show that for generating a specific torque or power in ISRM, less copper loss is produced compared to conventional SRM. Hence, not only the copper loss of the rotor of ISRM doesn't decrease the efficiency of ISRM, but also ISRM can be more efficient compared to conventional SRM. The efficiency of the ISRM and the efficiency of the conventional SRM at various output powers are calculated and presented in Fig. 16.

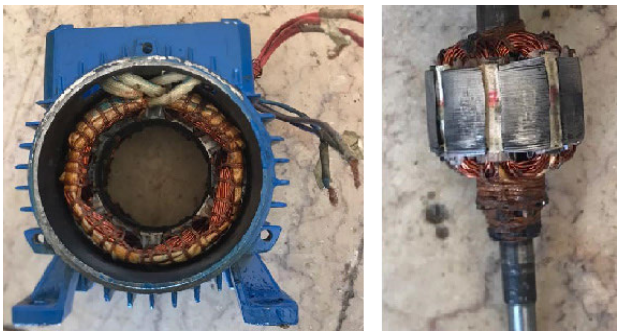

FIGURE 17. The stator and the rotor of the ISRM prototype.

TABLE 3. Cost analysis of the machines (ISRM and SRM).

Items	SRM	ISRM
Weight of electrical steel	15.3 *kg*	16.5 *kg*
Cost of electrical steel *(1.6 $/kg)*	*$*24.5	*$*26.4
Weight of copper	3.8 *kg*	7.8 *kg*
Cost of copper *(9 $/kg)*	*$*34.2	*$*70.2
Total cost *(steel + copper)*	*$*58.7	*$*96.6
Total weight *(steel + copper)*	19.1 *kg*	24.3 *kg*
Cost per N.m *(cost/T_{max})*	0.31 *$/N.m*	0.25 *$/N.m*

F. SPECIAL CARES

The cost analysis of the ISRM and the SRM is accomplished in this section. This analysis is only based on the cost of copper and electrical steel, and the results are presented in Table 3. Even though the ISRM is heavier and more expensive, it has lower cost per N.m (cost/T_{max}, compared to the SRM.

The previous studies on the SRMs with short flux path (such as Double Stator Switched Reluctance Machine) clarifies that this kind of SRMs have lower noise and vibration, compared to conventional SRMs [17]. But a comprehensive mechanical analysis is required to determine the actual noise and vibration of ISRM in a high-power experimental setup.

It should be mentioned that special methods should be considered for rotor cooling of ISRM. There are different modern heat extraction systems for electrical machines, that can be implemented to ISRM [19].

III. EXPERIMENTAL RESULTS

In order to evaluate the performance of the ISRM for EV application, a high power version of the machine should be developed and tested. But, because of the equipment and financial shortages, we had just the opportunity to build and test a simple low power ISRM in order to evaluate the preliminary performance of this motor. On the next step, by absorption of financial resources, we hope we would be able to design, build and test a high power ISRM with a modern cooling technique for real vehicle application.

Firstly, an ISRM prototype, with the specifications presented in Table 4, was built. The stator and the rotor lamination were made out of M19, using wire electrical discharge machining. The stator and the rotor of the ISRM are shown in Fig. 17. On the next step, an experimental setup was built as shown in Fig 18. The block diagram of the experimental test setup is illustrated in Fig. 19.

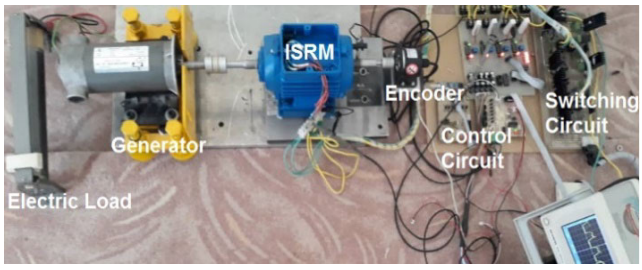

FIGURE 18. The experimental setup of the ISRM prototype.

TABLE 4. Characteristics of the ISRM prototype.

Stator Outer Radius	42.5 mm
Stack length	30 mm
Air gap	0.5 mm
Number of stator poles	12
Number of rotor poles	8
Turn number of stator coils	35
Turn number of rotor coils	35
Rated current	15 A
Maximum current Density	6 A/mm2
Rotor and stator material	M19
Rated power	500 W
Cooling method	natural cooling

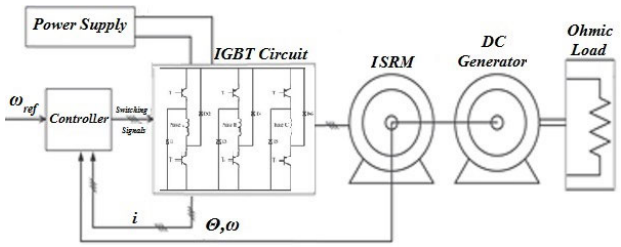

FIGURE 19. Block diagram of the experimental test setup of the ISRM.

In order to drive the ISRM, a couple of electronic boards were designed and implemented. In this test setup, a controller circuit was designed using Intel XMEGA32. This controller's task is to create sufficient gate pulses in order to turn on and turn off the IGBTs in the appropriate times.

The controller needs to have a reference speed, which is determined manually. The motor speed is calculated in the controller, using the position signal which is generated by the shaft encoder (E40S360, 360 pulses per round, incremental). The reference current is calculated by a PI controller, as shown in Fig. 19. Using a hysteresis current algorithm, the gate signals are generated and applied to the appropriate switches.

On the side of the power electronics, a full bridge converter was designed and built with six IXGH40N60 IGBTs and six RURG80100 diodes. Snubber circuits were designed for each switch in order to reduce the voltage stress on the IGBTs.

If both of the power switches on either side of the phase are turned on, then that corresponding phase will be excited. Once the current rises above the threshold value, the switches turn off. The energy stored within the motor winding maintains the current in the same direction, until that energy is depleted. If one phase is excited, the rotor rotates for 15 degrees (the stroke angle), from unaligned position

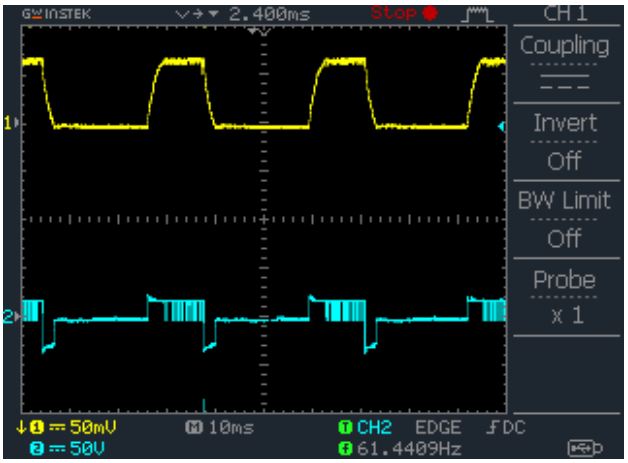

FIGURE 20. The phase current and voltage of the ISRM (300 rpm).

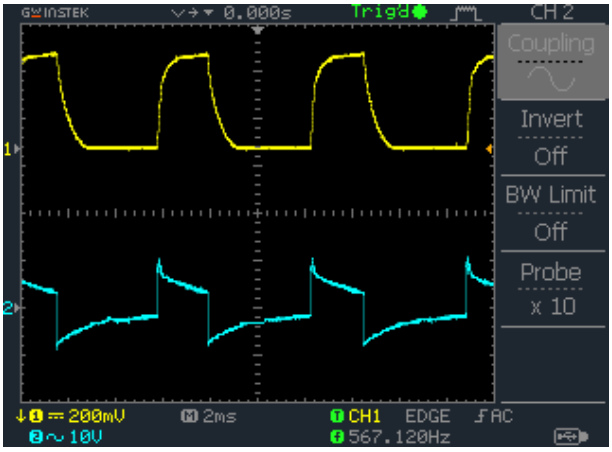

FIGURE 21. The phase current and voltage of the ISRM (1500rpm).

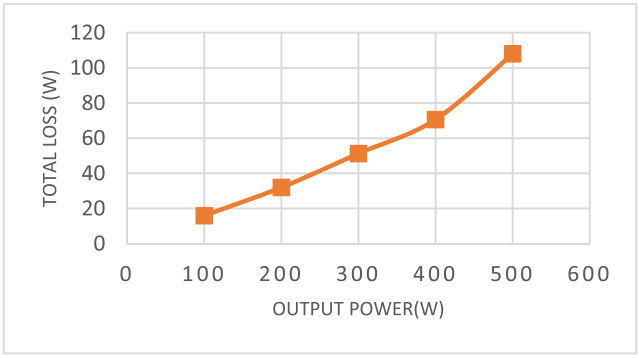

FIGURE 22. The total loss of the ISRM at various output powers (950 rpm).

towards aligned position. Continuing with the sequence of excitation, a counterclockwise excitation pattern of phases will result in a clockwise rotation, and vice versa.

Several tests in different currents and speeds were performed to observe the operation of the ISRM prototype. Fig. 20 shows a sample of the phase current and voltage at the speed of 300 rpm. At the low speeds, the hysteresis current control is implemented, but at the higher speeds (more than 1000 rpm), the hysteresis current controller is not required [18]. Fig. 21 shows a sample of the phase current and voltage at the speed of 1500 rpm.

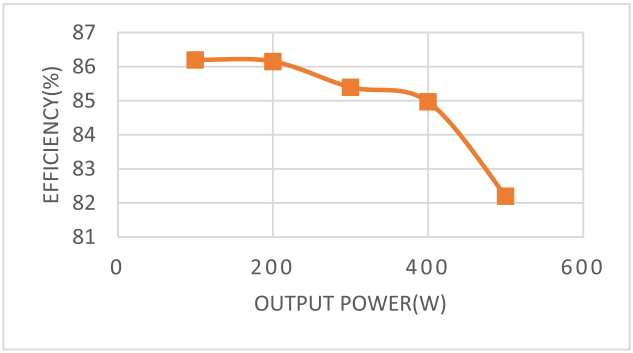

FIGURE 23. The efficiency of the ISRM at various output powers (950 rpm).

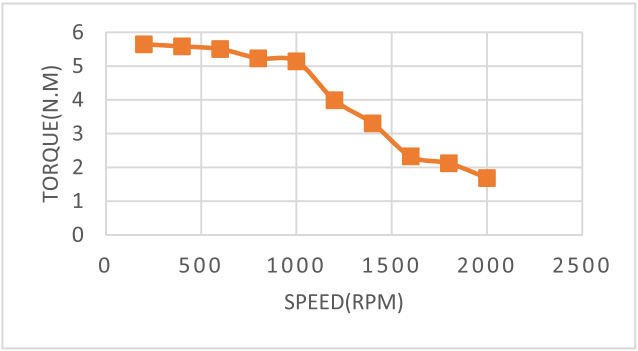

FIGURE 24. Torque versus speed of the ISRM.

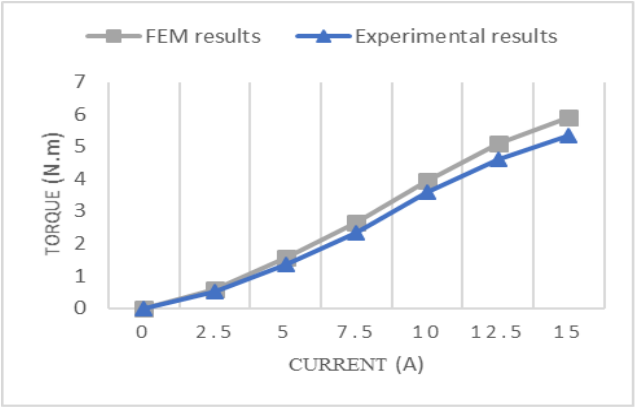

FIGURE 25. The FEM and the experimental results of the torque calculation (950 rpm).

By measuring the input power, the output power, and the speed of the ISRM prototype, it is possible to calculate the torque, the efficiency, and the total loss of the machine. The torque is derived, if the output power of the motor is divided by the motor speed. The efficiency is the output power divided by the input power, and the total loss is the input power minus the output power.

This ISRM prototype has a very low rated power. The efficiency of low-power ISRMs is low, compared to the efficiency of high-power ISRMs. The total loss and the efficiency of the ISRM is calculated for different output powers (at the speed of 950 rpm), and the results are presented in Fig. 22 and Fig. 23. In addition, torque versus speed of the ISM is illustrated in Fig. 24.

In order to evaluate the torque production of the ISRM prototype, the motor is also modeled and simulated using FEM. The calculated average torque (using FEM), along with the measured torque (using the experimental setup), at the speed of 950 rpm, and in different currents, are presented in Fig. 25. The results show a good agreement between the simulated and the experimental results. It should be mentioned that the poor rotor lamination has reduced the torque capability of the ISRM prototype.

IV. CONCLUSION

In this paper, Induction Switched Reluctance Machine (ISRM), was introduced for electric vehicle applications. In this electric machine, by placing coils on the rotor, a very short magnetic flux path is achieved, and an improvement in the torque capability of the machine is accomplished. In order to preliminary evaluation of ISRM, a 2D finite element model of the machine was created. Through comparison of an ISRM with a conventional SRM, it was demonstrated that the proposed ISRM exhibits a very good performance in terms of power and torque capability. Finally, a low power prototype of ISRM was built and tested and some motor quantities were measured and calculated. ISRM has a good potential to be implemented in electric vehicle propulsion system, since it has the following advantages: (1) ISRM has high torque density, and therefore provides high rate of vehicle acceleration. (2) ISRM can generate high power, and therefore eases the vehicle high-speed climbing. (3) ISRM has a wide high-efficiency operating area. (4) ISRM has high performance-to-price ratio. (5) ISRM can be driven using conventional SRM electric drives which has high reliability, and prevents short-circuit fault.

REFERENCES

[1] I. Boldea, L. N. Tutelea, L. Parsa, and D. Dorrell, "Automotive electric propulsion systems with reduced or no permanent magnets: An overview," *IEEE Trans. Ind. Electron.*, vol. 61, no. 10, pp. 231–239, Oct. 2014.

[2] P. Ramesh and N. C. Lenin, "High power density electrical machines for electric vehicles—Comprehensive review based on material technology," *IEEE Trans. Magn.*, vol. 55, no. 11, Nov. 2019, Art. no. 0900121.

[3] Y.-R. Kang, J.-C. Son, and D.-K. Lim, "Optimal design of IPMSM for fuel cell electric vehicles using autotuning elliptical niching genetic algorithm," *IEEE Access*, vol. 8, pp. 117405–117412, Jun. 2020.

[4] Z. Chen and G. Li, "A V type permanent magnet motor simulation analysis and prototype test for Electric vehicle," *IEEE Access*, vol. 7, pp. 174839–174846, Dec. 2019.

[5] J.-G. Lee, D.-K. Lim, and H.-K. Jung, "Analysis and design of interior permanent magnet synchronous motor using a sequential-stage magnetic equivalent circuit," *IEEE Trans. Magn.*, vol. 55, no. 10, pp. 411–420, Oct. 2019.

[6] H. Chen and C. H. T. Lee, "Parametric sensitivity analysis and design optimization of an interior permanent magnet synchronous motor," *IEEE Access*, vol. 7, pp. 159918–159929, Nov. 2019.

[7] Z. Yang, F. Shang, I. P. Brown, and M. Krishnamurthy, "Comparative study of interior permanent magnet, induction, and switched reluctance motor drives for EV and HEV applications," *IEEE Trans. Transport. Electrific.*, vol. 1, no. 3, pp. 245–254, Oct. 2015.

[8] A. Chiba, K. Kiyota, N. Hoshi, M. Takemoto, and S. Ogasawara, "Development of a rare-earth-free SR motor with high torque density for hybrid vehicles," *IEEE Trans. Energy Convers.*, vol. 30, no. 3, pp. 175–182, Mar. 2015.

[9] G. V. Kumar, C.-H. Chuang, M.-Z. Lu, and C.-M. Liaw, "Development of an electric vehicle synchronous reluctance motor drive," *IEEE Trans. Veh. Technol.*, vol. 69, no. 5, pp. 5012–5024, May 2020.

[10] A. Xu, C. Shang, J. Chen, J. Zhu, and L. Han, "A new control method based on DTC and MPC to reduce torque ripple in SRM," *IEEE Access*, vol. 7, pp. 68584–68593, 2019.

[11] J. Zhu, K. W. Cheng, X. Xue, and Y. Zou, "Design of a new enhanced torque in-wheel switched reluctance motor with divided teeth for electric vehicles," *IEEE Trans. Magn.*, vol. 53, no. 11, pp. 511–520, Nov. 2017.

[12] B. Fahim and M. Moallem, "Opportunities and challenges of switched reluctance motor drives for electric propulsion: A comparative study," *IEEE Trans. Transport. Electrific.*, vol. 3, no. 1, pp. 205–216, Oct. 2017.

[13] B. C. Mecrow, E. A. El-Kharashi, J. W. Finch, and A. G. Jack, "Preliminary performance evaluation of switched reluctance motors with segmental rotors," *IEEE Trans. Energy Convers.*, vol. 19, no. 4, pp. 679–686, Dec. 2004.

[14] M. M. J. Kondelaji and M. Mirsalim, "Segmented-rotor modular switched reluctance motor with high torque and low torque ripple," *IEEE Trans. Ind. Electron.*, vol. 6, no. 1, pp. 417–427, Dec. 2020.

[15] S. R. Mousavi-Aghdam, M. R. Feyzi, and N. Bianchi, "Design and analysis of a novel high-torque stator-segmented SRM," *IEEE Trans. Ind. Electron.*, vol. 63, no. 3, pp. 79–88, Dec. 2016.

[16] M. Abbasian, M. Moallem, and B. Fahimi, "Double-stator switched reluctance machines (DSSRM): Fundamentals and magnetic force analysis," *IEEE Trans. Energy Convers.*, vol. 25, no. 3, pp. 589–597, Sep. 2010.

[17] M. Abbasian, "Induction switched reluctance motor," U.S. Patent 2017 0 370 296 A1, Jun. 30, 2020.

[18] R. Krishnan, *Switched Reluctance Motor Drives: Modeling, Simulation, Analysis, Design, and Applications*. Boca Raton, FL, USA: CRC Press, 2001.

[19] I. Petrov, P. Lindh, M. Niemelä, E. Scherman, O. Wallmark, and J. Pyrhönen, "Investigation of a direct Liquid cooling system in a permanent magnet synchronous machine," *IEEE Trans. Energy Convers.*, vol. 35, no. 2, pp. 807–817, Jun. 2020.

MEYSAM AZAMIAN JAZI was born in Isfahan, Iran, in 1985. He received the bachelor's and M.Sc. degrees in electrical engineering from IAU University, Khorasgan, Isfahan, in 2010 and 2015, respectively, where he is currently pursuing the Ph.D. degree.

MOHAMMADALI ABBASIAN was born in Gaz, Isfahan, Iran. He received the bachelor's, M.Sc., and Ph.D. degrees in electrical engineering from the Isfahan University of Technology, in 2002, 2004, and 2011, respectively. From 2009 to 2010, he was a Ph.D. Exchange Student with Renewable Energies and Vehicular Technologies, The University of Texas at Arlington, Arlington, TX, USA. From 2017 to 2018, he was as a Research Scientist with Bundeswehr University, Munich, Germany. He is currently an Assistant Professor with IAU University, Khorasgan, Isfahn.

DIETER GERLING (Member, IEEE) was born in Menden/Sauerland, Germany, in 1961. He received the Diploma and Ph.D. degrees in electrical engineering from the Technical University of Aachen, Germany, in 1986 and 1992, respectively. From 1986 to 1999, he was with Philips Research Laboratories, Aachen, as a Research Scientist and later as a Senior Scientist. He joined Robert Bosch GmbH, Bühl, Germany, as the Director, in 1999. Since 2001, he has been a Full Professor with Bundeswehr University Munich, Neubiberg, Germany.